# Determination of Stress-intensity Factors for Cracks in Tubes Under Torsion

Results of a photoelastic investigation to determine the SIF's in thin cylindrical shells with arbitrarily oriented cracks subjected to torsion

by L.S. Srinath, N. Srinivasa Murthy and T.V. Hareesh

ABSTRACT—An experimental investigation by two-dimensional photoelastic technique is carried out to study the stress distribution and to determine the stress-intensity factors for arbitrarily oriented cracks in thin cylindrical shells subjected to torsion. A new method is employed to evaluate the pure and mixed-mode SIF's.

## Introduction

The determination of stress distributions in the near vicinity of arbitrarily oriented cracks in thin cylindrical shells subjected to pure torsion is of considerable importance in design practice. A study of the stress field near the crack tip provides valuable information, particularly regarding the stress-intensity factors. Depending upon the orientation of the crack, situations occur where the crack is subjected to either pure Mode I or pure Mode II, or to a combination of these modes.

The present paper describes the results of experimental investigations carried out on araldite tubes containing cracks oriented at 0 deg, 30 deg, 45 deg, 60 deg and 90 deg to the axis of the tube and subjected to pure torsion. The existing methods to determine the values of SIF's are not only sensitive to the measured parameters involved, but also do not yield either consistent or unique values. This is particularly so in the case of mixed-mode situations. The present paper describes a new method to evaluate the SIF's which yield unique and consistent values. The experimentally obtained values are compared with the limited theoretical results available. Furthermore, a flat plate containing a crack was loaded in such a manner so as to produce a pure Mode II situation, and the value of nondimensionalized SIF obtained for such a model is compared with the values obtained for the tubes.

## Experimental Details

### *Thin Shell Specimens*

Araldite tubes cold cast from CY 230 resin and HY 951 hardener manufactured by M/s. Ciba-Geigy of India Ltd. were finished to the dimensions shown in Fig. 1. Slits, 24-mm long and 0.4-mm wide, were cut in these tubes using a HSS slitting saw to simulate through cracks. With reference to the axis of the tubes, the crack orientations $\alpha$ were 0 deg, 30 deg, 45 deg, 60 deg and 90 deg. Precautions were taken to see that the residual stresses near the crack tips were negligible. Using a suitable loading fixture, the tubes were subjected to pure torsion. All tubes were subjected to the same torsional moment. The magnitude of the shear stress induced in regions far from the crack zone was found theoretically as well as experimentally to be equal to 14.2 kgf/cm$^2$.

In order to employ photoelastic techniques, a small unit containing a polarizer and a quarter-wave-plate combination was inserted into the tube. The tube with the insertion was immersed in a liquid having the same refractive index as the tube material. The second quarter wave plate and the analyzer were kept outside the tube. A schematic arrangement of this setup is shown in Fig. 2. Fringe patterns near the crack tips corresponding to dark and bright fields were recorded on photographic film and blown up for analyses. The material fringe value for the shell material was determined as 12 kgf per-cm per-fringe.

### *Two-dimensional Plate Model*

A two-dimensional plate model, as shown in Fig. 3, was employed to develop a Mode II stress field at the crack tip. A specially constructed loading frame which prevents the development of an opening-mode situation by providing side constraints was employed to obtain a pure Mode II situation. The load applied on the specimen was 45.5 kgf. The material-fringe value for the plate specimen was found to be 11.2 kgf per-cm per-fringe.

## Fringe Patterns Observed

Figures 4-8 show the dark-field fringe patterns for crack orientations of 0 deg, 90 deg, 30 deg, 45 deg and 60 deg, respectively. Choosing rectangular axes that are along and perpendicular to the crack orientations, the rectangular stress components existing in the shell in the absence of a crack are shown in Figs. 9(a)-(e). Figure 10 shows the fringe pattern for the two-dimensional plate model.

From the fringe patterns obtained one can observe the following:

*L.S. Srinath, N. Srinivasa Murthy and T.V. Hareesh are Professor, Assistant Professor and Graduate Student, respectively, Department of Mechanical Engineering, Indian Institute of Science, Bangalore, India.*

*Original manuscript submitted: November 24, 1982. Authors notified of acceptance: February 1, 1983. Final version received: March 4, 1983.*

(1) For crack orientations of $\alpha = 0$ deg and 90 deg, the fringe patterns are identical and these agree with the computer plots of maximum-shear-stress lines of a Mode II crack obtained by Sanford and Dally.[1] The far-field state of stress for both of these two cases is one of pure shear as shown in Figs. 9(a) and (b).

(2) The fringe pattern observed in the case of the plate model is similar to those obtained for the shell models with crack orientations of $\alpha = 0$ deg and 90 deg.

(3) For crack orientations of $\alpha = 30$ deg, 45 deg and 60 deg, mixed-mode situations exist. The far-field state of stress for these are shown in Figs. 9(c)-(e). It is important to observe that though the far-field stress for $\alpha = 45$ deg is one of pure tension and compression, a mixed-mode situation exists because of the curvature effect of the shell. This is revealed by the stress pattern and also substantiated by the theoretical analysis of Lakshminarayana, Murthy and Srinath.[2]

(4) For mixed-mode situations, the isochromatic-fringe loops on one side of the crack are bigger than the fringe loops on the other side.

(5) Comparing the fringe patterns for $\alpha = 30$ deg and $\alpha = 60$ deg with respect to that for $\alpha = 45$ deg, the size and tilt of the loops on either side of the crack axis follows the far-field shear-stress directions, i.e., for $\alpha = 30$ deg, the larger loop is on the right side of the crack axis, whereas for $\alpha = 60$ deg, it is on the left of the crack axis. The far-field shear-stress directions as shown in Figs. 9(c) and (e) correspond to these.

The apogee angles of the larger loops for $\alpha = 30$ deg and $\alpha = 60$ deg are equal ($\simeq$52 deg with respect to their crack axes). So also are the apogee angles of the smaller loops ($\simeq$91 deg).

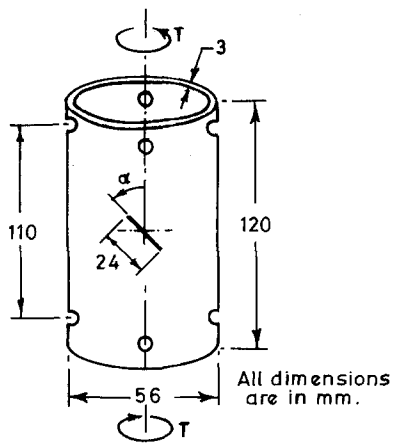


Fig. 1—Dimensions of the shell with crack under torsion

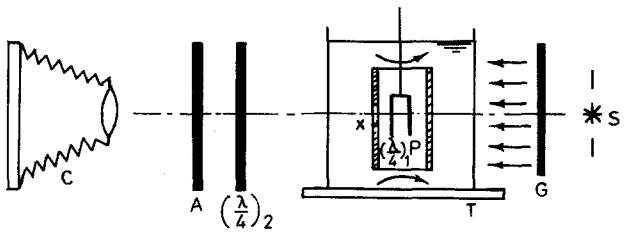


S: Source of monochromatic light, G: Ground glass plate, T: Tank filled with refractive index matching liquid, P: Polarizer $(\lambda/4)_1$: I Quarter wave plate, $(\lambda/4)_2$: II Quarter wave plate, A: Analyser, C: Camera, x: Crack on the tube specimen.

Fig. 2—The schematic diagram of the polariscope

## Evaluation of SIF's

### *Pure-shear-mode Situations*

The fringe patterns shown in Figs. 4, 5 and 10 correspond to pure Mode II situations. Westergaard's equations for the stresses in the immediate vicinity of the crack tip are

$$\begin{bmatrix} \sigma_x \\ \sigma_y \\ \tau_{xy} \end{bmatrix} = \frac{K_2}{\sqrt{2\pi r}} \begin{bmatrix} -\sin\frac{\theta}{2}\left(2+\cos\frac{\theta}{2}\cos\frac{3\theta}{2}\right) \\ \sin\frac{\theta}{2}\cos\frac{\theta}{2}\cos\frac{3\theta}{2} \\ \cos\frac{\theta}{2}\left(1-\sin\frac{\theta}{2}\sin\frac{3\theta}{2}\right) \end{bmatrix} \quad (1)$$

From these, calculating the maximum shear stress $\tau_m$, one gets

$$\tau_m = \sqrt{\left[\left(\frac{\sigma_x - \sigma_y}{2}\right)^2 + \tau_{xy}^2\right]}$$

$$= \frac{K_2}{\sqrt{2\pi r}} \sqrt{[\cos^2\theta + \tfrac{1}{4}\sin^2\theta]} \quad (2a)$$

$$= \frac{NF}{(2t)} \quad (2b)$$

where

$N$ = fringe order
$F$ = material-fringe constant
$t$ = thickness of the specimen

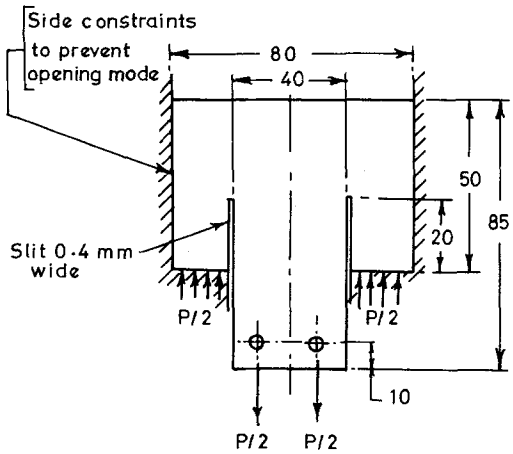


Fig. 3—Dimensions of the plate model subjected to Mode II deformation

$(r, \theta)$ are the usual polar coordinates measured from the tip of the crack as shown in Fig. 11.

While there is no standard method established to evaluate $K_2$ for pure Mode II situations, conceivably one can use directly Westergaard's eq (1) and utilize Irwin's concept in identifying the point where $\partial \tau_m / \partial \theta = 0$. This is the technique adopted by Smith and Smith.[3] However, the values of $K_2$ obtained by such a method are not only very sensitive to the measured parameters $r$ and $\theta$, but also do not yield a unique value. One of the reasons for this is the fact that Westergaard's equations as given by eq (1) are strictly valid in the immediate vicinity of the crack tip, and invariably in all experiments a nonlinear elastic-plastic stress field exists near the crack tips. Consequently, eq (1) requires modifications to take care of this aspect. Further, when photoelastic observations are used to calculate the values of SIF's, measurements are made at points or zones which are not in the immediate vicinity of the crack tip. This also necessitates modifications of eq (1). Following Ref. 4, the stress field in the not-too-near vicinity of the crack tip is expressed as

$$\sigma_1 - \sigma_2 = \frac{NF}{t} = \frac{K}{\sqrt{(r/a)}} + \sum_{m=1}^{M} B_m \left(\frac{r}{a}\right)^m \quad (3)$$

where

$$K = \frac{2K_2}{\sqrt{2\pi a}} \sqrt{[\cos^2 \theta + \tfrac{1}{4} \sin^2 \theta]} \quad (4)$$

In the present investigation, it was found sufficient to use only the first term in the summation part, i.e., $B_1 \left(\frac{r}{a}\right)$. Calculations showed that the value of $B_2 \left(\frac{r}{a}\right)^2$ was inconsequential. It is important to observe that the constants $B_1, B_2, \ldots\ldots B_m$ and the value of $K$ in eq

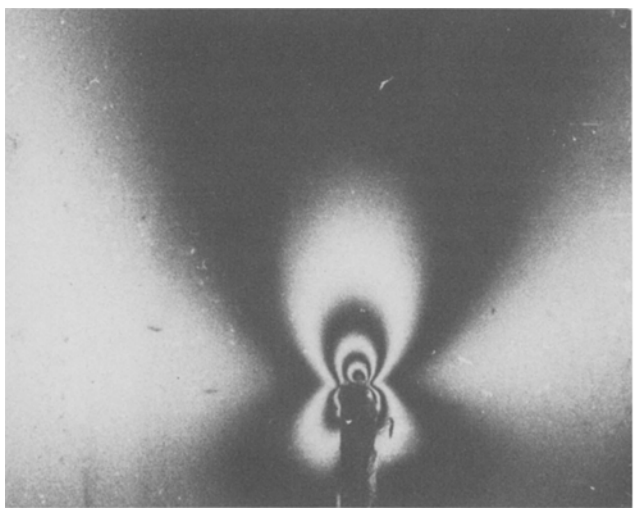

Fig. 4—Isochromatic pattern for a crack at 0 deg to the shell axis

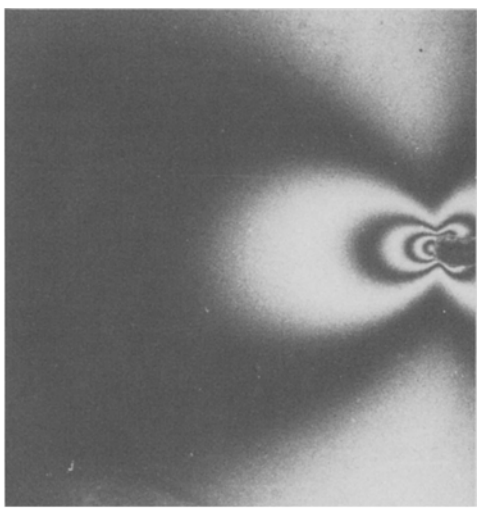

Fig. 5—Isochromatic pattern for a crack at 90 deg to the shell axis

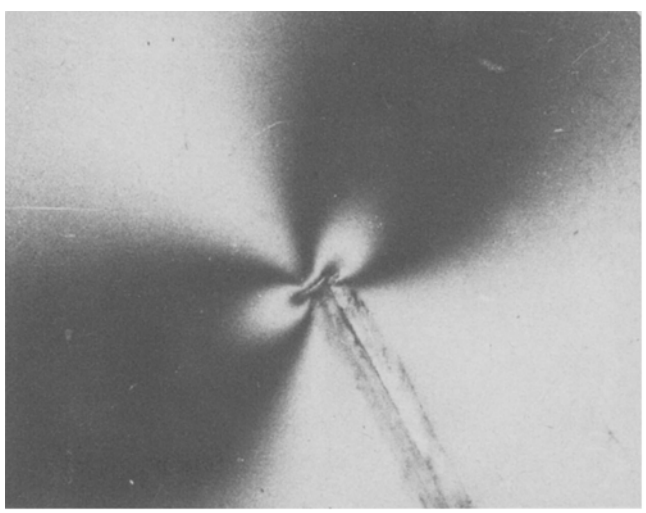

Fig. 6—Isochromatic pattern for a crack at 30 deg to the shell axis

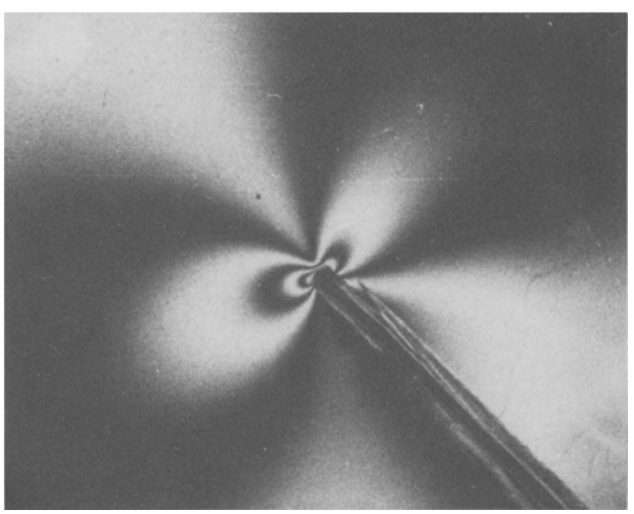

Fig. 7—Isochromatic pattern for a crack at 45 deg to the shell axis

(3), depend on $\theta$. Choosing only $B_1$, eq (3) becomes for two points $r_1$ and $r_2$ along a line $\theta$

$$\frac{N_1F}{t} = \sigma_1 - \sigma_2 = \frac{K}{\sqrt{(r_1/a)}} + B_1(r_1/a)$$
$$\frac{N_2F}{t} = \sigma_1 - \sigma_2 = \frac{K}{\sqrt{(r_2/a)}} + B_1(r_2/a) \quad (5)$$

Solving the above two equations simultaneously, the values of $K$ and $B_1$ can be determined. From eq (4), the value of $K_2$ can be evaluated. The values of $K_2$ so determined from eqs (5) and (4) are found to be consistent. The value of $K_2$ for the shell models ($\alpha$ = 0 deg and 90 deg) was 43.8 kgf cm$^{-3/2}$.

Equation (5) was used to evaluate $K_2$ for the plate model also. The value obtained was 37.5 kgf cm$^{-3/2}$. In order to compare the values of $K_2$ obtained for the shell model and the plate model, these values were nondimensionalized. The value of $K_2$ for the shell model was divided by $\tau_t\sqrt{a_t}$ where $\tau_t$ is the nominal shear stress induced by the torque and $a_t$ was half the crack length. For the plate model, the dividing factor was $\tau_p\sqrt{a_p}$, where $\tau_p$ was the average shear stress induced by the load $P$. The nondimensionalized values were 2.83 and 2.78 respectively for the shell and plate models. Further, the SIF value for the plate model was compared with the analytically obtained SIF from the boundary collocation technique of Jones and Chisholm.[5,6] The difference was found to be within five percent.

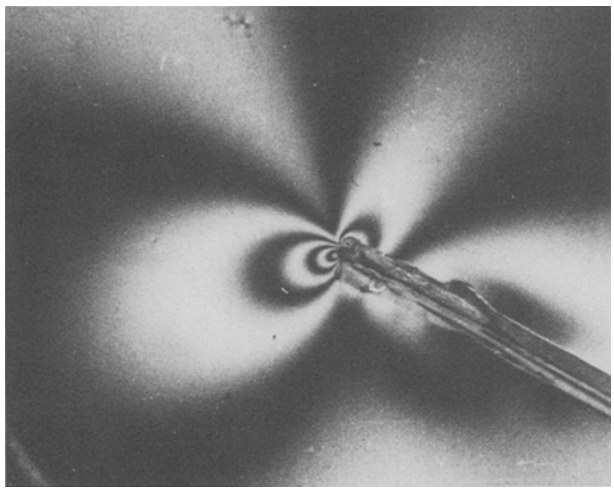

Fig. 8—Isochromatic pattern for a crack at 60 deg to the shell axis

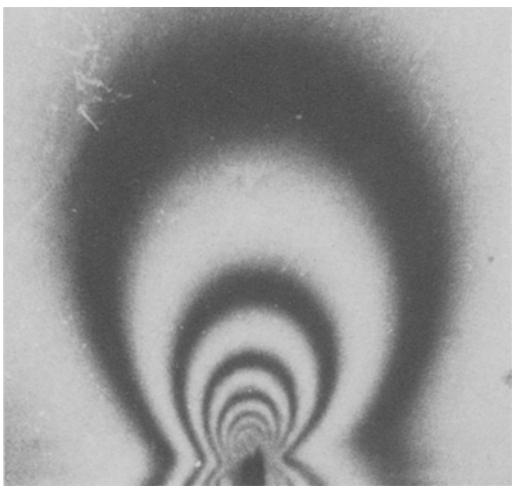

Fig. 10—Isochromatic patterns for the plate model with crack under pure Mode II deformation

### Mixed-mode Situations

For shells with crack orientations $\alpha$ = 30 deg, 45 deg and 60 deg, mixed-mode situations exist. Westergaard's equations for combined mode are

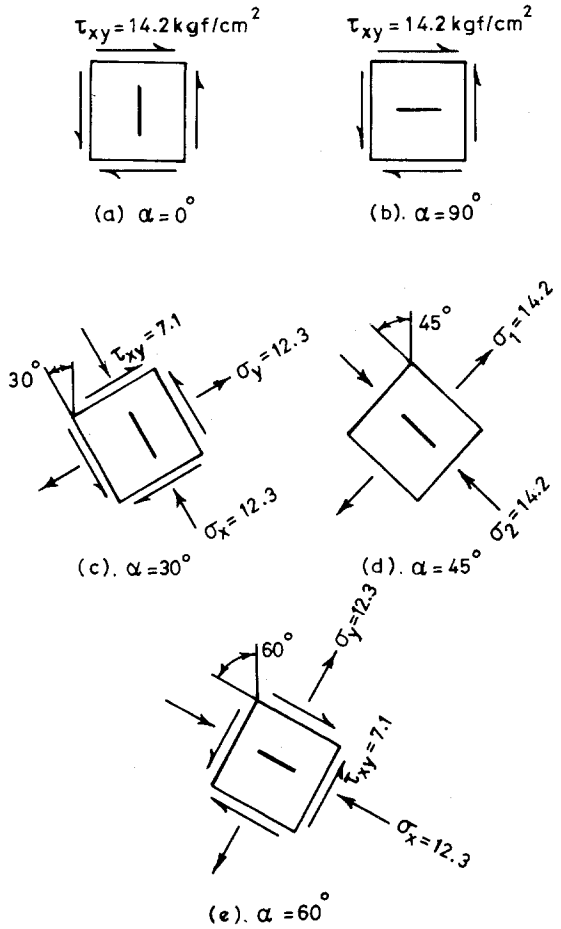


Fig. 9—Different states of stress for $\alpha$ equal to 0 deg, 90 deg, 30 deg, 45 deg and 60 deg

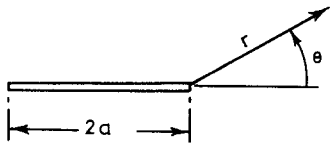


Fig. 11—Polar-coordinate representation of a point in the field with respect to the crack tip

$$\begin{bmatrix}\sigma_x\\ \sigma_y\\ \tau_{xy}\end{bmatrix} = \frac{K_1}{\sqrt{2\pi r}}\begin{bmatrix}\cos\frac{\theta}{2}\left(1-\sin\frac{\theta}{2}\sin\frac{3\theta}{2}\right)\\ \cos\frac{\theta}{2}\left(1+\sin\frac{\theta}{2}\sin\frac{3\theta}{2}\right)\\ \cos\frac{\theta}{2}\sin\frac{\theta}{2}\cos\frac{3\theta}{2}\end{bmatrix} + \frac{K_2}{\sqrt{2\pi r}}\begin{bmatrix}-\sin\frac{\theta}{2}\left(2+\cos\frac{\theta}{2}\cos\frac{3\theta}{2}\right)\\ \sin\frac{\theta}{2}\cos\frac{\theta}{2}\cos\frac{3\theta}{2}\\ \cos\frac{\theta}{2}\left(1-\sin\frac{\theta}{2}\sin\frac{3\theta}{2}\right)\end{bmatrix} \quad (6)$$

from these, one gets

$$\frac{\sigma_1-\sigma_2}{2} = \tau_m = \frac{1}{2\sqrt{2\pi r}}\sqrt{[(K_1\sin\theta+2K_2\cos\theta)^2+(K_2\sin\theta)^2]}$$

Similar to the pure-mode situation, the above equation is modified for the not-too-near vicinity of the crack tip as

$$\sigma_1-\sigma_2 = \frac{NF}{t} = \frac{K}{\sqrt{(r/a)}} + \sum_{m=1}^{M} B_m(r/a)^m \quad (7)$$

where

$$K = \frac{1}{\sqrt{2\pi a}}\sqrt{[(K_1\sin\theta+2K_2\cos\theta)^2+(K_2\sin\theta)^2]} \quad (8)$$

Here also, the values of $K$ and $B_m$ are functions of $\theta$. Once again retaining only $B_1$ in eq (7), the values of $K$ and $B_1$ can be determined by choosing two points $r_1$ and $r_2$ along a line $\theta$. Since $K$ is a function of $K_1$ and $K_2$, another set of values $K'$ and $B_1'$ are determined along a second line $\theta'$. From these values of $K$ and $K'$, the values of $K_1$ and $K_2$ are determined. The values of $K_1$ and $K_2$ so obtained are found to satisfy the equation for any third line $\theta''$ also. Again, eq (7) yields consistent values for $K_1$ and $K_2$ for each $\alpha$. Table 1 gives the results obtained.

Figures 12 and 13 show the variations of nondimensional SIF's, theoretical and experimental, $K_1/(\tau_t\sqrt{a_t})$ and $K_2/\tau_t\sqrt{a_t}$), as functions of the crack-orientation angle $\alpha$. Though the number of points obtained from the present investigation are limited, the mode of variations are similar to the theoretical curves of Ref. 2. The theoretical solutions are available for shells having a curvature parameter $\beta$, $0 \le \beta \le 1$. This curvature parameter is a nondimensional quantity defined as

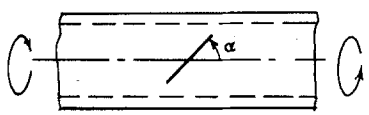


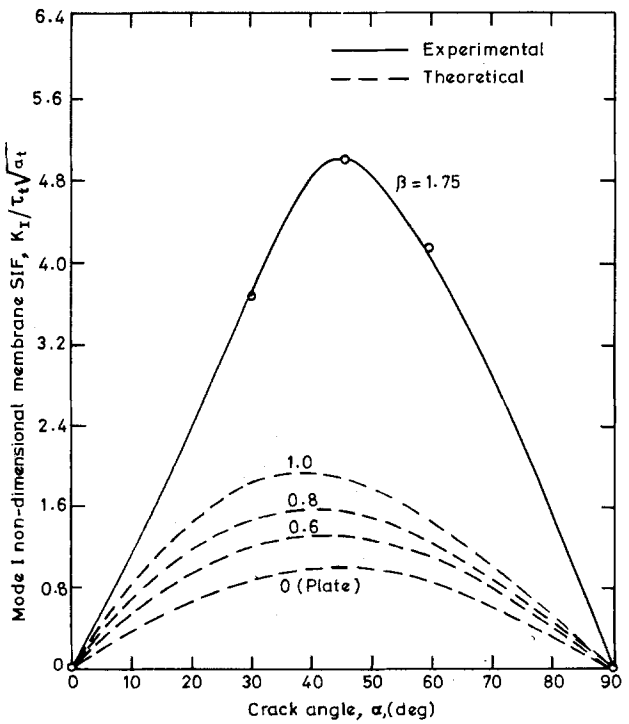


Fig. 12—Plot of nondimensional Mode I SIF, theoretical and experimental, vs. $\alpha$

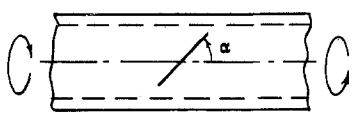


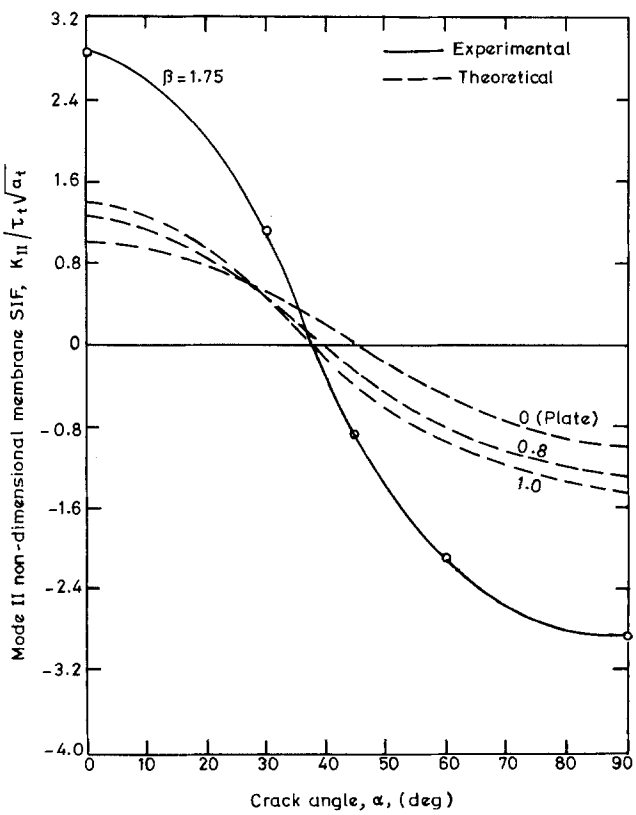


Fig. 13—Plot of nondimensional Mode II SIF, theoretical and experimental, vs. $\alpha$

$$\beta = \frac{a}{\sqrt{8Rt}} [12(1 - \nu^2)]^{1/4}$$

where

$2a$ = crack length
$R$ = radius of shell
$t$ = thickness of shell
$\nu$ = Poisson's ratio

For our shell models, $\beta = 1.75$.

## Conclusions

The present investigation is concerned with the determination of SIF's for arbitrarily oriented cracks in shells subjected to pure torsion. The crack orientations tested were at angles of $\alpha$ equal to 0 deg, 30 deg, 45 deg, 60 deg and 90 deg with respect to the shell axis. In addition to the shell model, a two-dimensional plate with cracks was suitably loaded to induce pure Mode II situation. The values of $K_1$ and $K_2$ were determined by using modified Westergaard's equations as proposed by Prabhu *et al.*[4] so that the measurements made in the not-too-near zones of the crack tips yield consistent and unique values. The values of nondimensionalized $K_2$ obtained for cracks with $\alpha = 0$ deg and $\alpha = 90$ deg compare very well with those obtained for the plate model. For cracks with $\alpha = 30$ deg, 45 deg and 60 deg, mixed-mode situations exist and the values of $K_1$ and $K_2$ obtained by the new method are again consistent. An error analysis shows that errors of $\pm 3$ deg made in the measurement of $\theta$ result in values of $K_1$ not differing by more than $\pm 0.15$ percent and $K_2$ not differing by more than $\pm 4$ percent. The design parameter $(K_1^2 + K_2^2)/E$ does not vary by more than 0.25 percent. The variations of $K_1$ and $K_2$ as functions of $\alpha$ have the same mode shape as those obtained analytically. In the present investigation only the first term of the series was used. Though it is conceivable that truncation with only a finite number of terms might not work for a general geometry, it is observed in the present series of investigations that truncating with only the first term of the series has given consistent results.

In all the investigations a narrow slit was used instead of a crack. According to Smith *et al.*[7] the use of a slit can have a consistent effect of raising the measured stress-intensity factor. However the plate model with a narrow slit of 0.4-mm width subjected to pure Mode II deformation gives values for SIF which agree with the SIF analytically obtained by the boundary-collocation techniques of Jones and Chisholm[5,6] within five percent. The shell model under torsion having a 0-4-mm wide slit oriented at $\alpha$ equal to 0 deg and 90 deg and hence subjected to pure Mode II deformation resulted in nondimensional SIF's which agree quite well with those for the plate model. Hence it can be construed that a narrow slit is representative of a crack to a fair degree of accuracy.

## References


1. *Dally, J.W. and Sanford, R.J., "Classification of Stress-intensity Factors from Isochromatic-fringe Patterns,"* EXPERIMENTAL MECHANICS, **18** *(12), 441-448 (1978).*
2. *Lakshminarayana, H.V., Murthy, M.V.V. and Srinath, L.S., "On a Finite Element Model for the Analysis of Through Cracks in Laminated Anisotropic Cylindrical Shells," J. Engrg. Fract. Mech.,* **14** *(4), 697-712 (1981).*
3. *Smith, D.G. and Smith, C.W., "Photoelastic Determination of Mixed Mode SIFs," J. Engrg. Fract. Mech.,* **4** *(2), 357-366 (1972).*
4. *Prabhu, M.M., Godbole, P.D., Bhave, S.K. and Srinath, L.S., "Modified Approach for Determining Stress Intensity Factor in SEN Specimen Using Photoelasticity," Proc. 1982 Joint Conf. Exper. Mech. (SESA/JSME), Hawaii, May 22-30, 1982.*
5. *Jones, D.L. and Chisholm, D.B., "An Investigation of Edge Sliding Mode in Fracture Mechanics," J. Engrg. Fract. Mech.,* **7**, *261-270 (1975).*
6. *Chisholm, D.M. and Jones, D.L., "An Analytical and Experimental Stress Analysis of a Practical Mode II Fracture Test Specimen,"* EXPERIMENTAL MECHANICS, **17** *(1), 7-13 (1977).*
7. *Smith, C.W., McGowan, J.J. and Jolles, M., "Effects of Artificial Cracks and Poisson's Ratio Upon Photoelastic Stress-intensity Determination,"* EXPERIMENTAL MECHANICS, **16** *(5), 188-193 (1976).*


**TABLE 1**

| $\alpha = 30^\circ$ | | | | $\alpha = 45^\circ$ | | | | $\alpha = 60^\circ$ | | | |
|---|---|---|---|---|---|---|---|---|---|---|---|
| | | $\sigma_1 - \sigma_2$ 40 kgf.cm$^{-2}$ | $\sigma_1 - \sigma_2$ 60 kgf.cm$^{-2}$ | | | $\sigma_1 - \sigma_2$ 40 kgf.cm$^{-2}$ | $\sigma_1 - \sigma_2$ 60 kgf.cm$^{-2}$ | | | $\sigma_1 - \sigma_2$ 40 kgf.cm$^{-2}$ | $\sigma_1 - \sigma_2$ 60 kgf.cm$^{-2}$ |
| | | r/a | r/a | | | r/a | r/a | | | r/a | r/a |
| $\theta$ | $90^\circ$ | 0.352 | 0.132 | $\theta$ | $90^\circ$ | 0.856 | 0.24 | $\theta$ | $90^\circ$ | 0.914 | 0.485 |
| $\theta'$ | $54^\circ$ | 0.608 | 0.176 | $\theta'$ | $50^\circ$ | 0.705 | 0.23 | $\theta'$ | $10^\circ$ | 0.608 | 0.220 |
| $\theta''$ | $45^\circ$ | 0.586 | 0.154 | $\theta''$ | $25^\circ$ | 0.352 | 0.115 | $\theta''$ | $20^\circ$ | 0.784 | 0.291 |
| $K_1$ kgf.cm$^{-3/2}$ | | 55.8 | | | | 75.6 | | | | 63.6 | |
| $K_2$ kgf.cm$^{-3/2}$ | | 16.8 | | | | 13.4 | | | | 32.2 | |

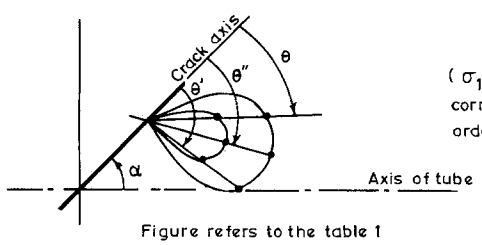


($\sigma_1 - \sigma_2$) of 40 and 60 kgf.cm$^{-2}$ correspond respectively to fringe orders of 1 and 1.5

Figure refers to the table 1